Challenging cosmic ray propagation with antiprotons.
Evidence for a "fresh" nuclei component?

Igor V. Moskalenko[1]

NASA/Goddard Space Flight Center, Code 660, Greenbelt, MD 20771

imos@milkyway.gsfc.nasa.gov

Andrew W. Strong

*Max-Planck-Institut für extraterrestrische Physik, Postfach 1603, D-85740 Garching,
Germany*

aws@mpe.mpg.de

Stepan G. Mashnik

Theoretical Division, Los Alamos National Laboratory, Los Alamos, NM 97545

mashnik@t2y.lanl.gov

and

Jonathan F. Ormes

NASA/Goddard Space Flight Center, Code 600, Greenbelt, MD 20771

jfo@lheapop.gsfc.nasa.gov

ABSTRACT

Recent measurements of the cosmic ray (CR) antiproton flux have been shown to challenge existing CR propagation models. It was shown that the reacceleration models designed to match secondary to primary nuclei ratio (e.g., Boron/Carbon) produce too few antiprotons, while the "traditional" non-reacceleration models can reproduce the antiproton flux but fall short of explaining the low-energy decrease in the secondary to primary nuclei ratio. Matching

---

[1]Joint Center for Astrophysics, University of Maryland, Baltimore County, Baltimore, MD 21250

both the secondary to primary nuclei ratio and antiproton flux requires artificial breaks in the diffusion coefficient and the primary injection spectrum suggesting the need for other approaches.

In the present paper we discuss one possibility to overcome these difficulties. Using the measured antiproton flux to fix the diffusion coefficient, we show that the spectra of primary nuclei as measured in the heliosphere may contain a fresh local "unprocessed" component at low energies, thus decreasing the measured secondary to primary nuclei ratio. A model reproducing antiprotons, B/C ratio, and abundances up to Ni is presented.

Subject headings: diffusion — convection — elementary particles — nuclear reactions, nucleosynthesis, abundances — cosmic rays — ISM: general — Galaxy: general — cosmology: theory — dark matter

1. Introduction

The spectrum and origin of antiprotons in CR has been a matter of active debate since the first antiproton detection in ballon flights was reported (Golden et al. 1979; Bogomolov et al. 1979). Because of the baryonic asymmetry of the Universe, antiprotons hardly occur at rest. There is a consensus that most of the CR antiprotons observed near the Earth are secondaries produced in collisions of energetic CR particles with interstellar gas (e.g., Mitchell et al. 1996).

The spectrum of secondary antiprotons has a peak at about 2 GeV decreasing sharply towards lower energies. This unique shape distinguishes antiprotons from other cosmic-ray species and allows for searches of primary antiprotons at low energies. Over the last years sufficient accuracy has been reached in measurements of the antiproton flux (BESS 1995-2000, Orito et al. 2000; Sanuki et al. 2000; Asaoka et al. 2002) to allow us to test Galactic CR propagation models, heliospheric modulation, and better restrict the spectrum of the secondary component.

It has been recently shown (Moskalenko et al. 2002) that accurate antiproton measurements during the last solar minimum 1995-1997 (BESS, Orito et al. 2000) challenge existing propagation models. In particular, the conventional models based on local CR measurements, simple energy dependence of the diffusion coefficient, and uniform CR source spectra throughout the Galaxy fail to reproduce simultaneously both, secondary to primary nuclei ratio and antiproton flux.

The reacceleration model designed to match secondary to primary nuclei ratio (e.g.,

Boron/Carbon) produces too few antiprotons because matching the B/C ratio at all energies requires the diffusion coefficient to be too large. The non-reacceleration models can reproduce the antiproton flux while fall short of explaining the low-energy decrease in the secondary to primary nuclei ratio. To be consistent with both, the introduction of breaks in the diffusion coefficient and the injection spectrum is required, which would indicate new phenomena in particle acceleration and propagation.

Recently there has appeared some indication that the atmospheric contribution to the antiproton flux measured in the upper atmosphere is underestimated. If this is true, the reacceleration model could still be the best one to describe propagation of nucleon species in the Galaxy (for more details see Section 4). However, in this work we have assumed the correctness of the published Galactic antiproton fluxes.

In the present paper we discuss another possibility to overcome the difficulties encountered by reacceleration models: a local primary component at low energies, perhaps associated with the Local Bubble.

2. Interstellar Cosmic Ray Spectrum

Just as secondary nuclei are abundant in CR and rare in the interstellar medium (ISM), since they are the product of the disintegration of primary nuclei, diffuse continuum γ-rays, antiprotons, and positrons are secondary products of interactions of mostly CR protons and He nuclei with interstellar gas. The CR propagation model which describes the secondary to primary ratio should equally well describe, e.g., B/C, sub-Fe/Fe, $\bar{p}/p$ ratios, and spectra of nuclei, positrons, and diffuse γ-rays.

The diffusive reacceleration models naturally reproduce secondary to primary nuclei ratios in CR and agree better with K-capture parent/daughter nuclei ratio (e.g., see Jones et al. 2001), though this result is not completely conclusive due to the large error bars in CR measurements and uncertainties in important isotopic cross sections. It is, however, clear that some reacceleration is unavoidable in the interstellar medium. Because of the unique shape of the antiproton spectrum, the effect of reacceleration is much weaker here than in the case of nuclei; since their production spectrum can be calculated accurately, antiprotons provide a useful tool to test propagation models (and heliospheric modulation).

Our previous result (Moskalenko et al. 2001b, 2002), in agreement with calculations of other authors (Molnar & Simon 2001), was that matching the secondary/primary nuclei ratio B/C using reacceleration models leads to values of the spatial diffusion coefficient apparently too large to produce the required antiproton flux, when the propagated nucleon spectra are

tuned to match the local proton and He flux measurements. This is an essential shortcoming.

Assuming the measured antiproton flux is correct and the current heliospheric modulation models are approximately right, we have the following possibility to reconcile the B/C ratio with the required flux of secondary antiprotons. The spectra of primary nuclei as measured in the heliosphere may contain a fresh local "unprocessed" component at low energies thus decreasing the measured secondary to primary nuclei ratio. This component would have to be local in the sense of being specific to the solar neighbourhood, so that the well-known "Local Bubble" phenomenon is a natural candidate.

The idea that CR are accelerated out of SN ejecta-enriched matter in superbubbles has been discussed in numerous papers (e.g., Higdon, Lingenfelter, & Ramaty 1998, and references therein). The possibility that the fresh component is coming from the Local Bubble (LB) has been discussed by, e.g., Morfill & Freyberg (1998) and Davis et al. (2000). We will further call it as the "Local Bubble Hypothesis." The idea is that primary CR like ^{12}C and ^{16}O have a local component at low energies, while secondary CR like B are produced Galaxy-wide over the confinement time of 10–100 Myr. Then the B/C ratio will be lower at low energies than expected in a uniform model, due to the enhanced local C (and the reduced Galactic production of B). If this idea is correct then the high-energy part of the secondary/primary nuclei ratio plus the measured antiproton flux at maximum, ~ 2 GeV, can be used to restrict the value and energy dependence of the diffusion coefficient, while the required contribution of the local sources can be derived from the measured secondary/primary nuclei ratio at low energies.

One additional hint for the possible existence of an "unprocessed" component is the calculated ratio of $C^{13}/C^{12} \sim 0.14$ at 200 MeV/nucleon (modulation potential 500 MV), which appears to be a factor of two larger than that observed 0.0629 ± 0.0023 (Lukasiak et al. 1994), 0.0588 ± 0.0013 (Connell 2001) when the propagation parameters are tuned to the B/C ratio (Moskalenko et al. 2002). The isotope C^{13} is almost whole secondary, as for Be and B isotopes. Since the primary source of C^{13} is O^{16}, accounting for as much as $\sim 60\%$ of the total, this may indicate an "over-enrichment" of the assumed source abundances in Oxygen. If so, the "over-enrichment" may be true also for primary Carbon, but tuning to the observed B/C artificially eliminates the excess of Lithium, Beryllium, and Boron. We note that the ratio of N^{15}/O^{16} is, however, correct, and the problem with overproduction of C^{13} may arise from cross section errors [2] (see Appendix).

---

[2]The production cross sections of $N^{14,15}$, and $C^{12,13}$ have been measured only in a narrow energy range.

3. Local Bubble Hypothesis

The low-density region around the Sun filled with hot H I gas is called the Local Bubble (e.g., Sfeir et al. 1999). The size of the region is about 200 pc, and it is likely that it was produced in a series of SN explosions. The most probably progenitor was an OB star association. Though people discuss different scenarios (e.g., Maíz-Apellániz 2001; Berghöfer & Breitschwerdt 2002), the LB age and the number of SN progenitors appears to be similar, ~ 10 Mys and $\sim 10 - 20$ SN, correspondingly. Most probably they exploded as core-collapse SN II or thermonuclear SN Ib/c with a mass of pre-SN stars between several and $\sim 10 M_\odot$, with the last SN explosion occuring approximately 1–2 Myr ago, or 3 SNe occuring within the last 5 Myr.

There is also some evidence of a SN explosion nearby. An excess of ^{60}Fe measured in a deep ocean ferromanganese crust suggests the deposition of SN produced iron on earth (Knie et al. 1999). The enhanced concentrations were found in two of three layers corresponding to a time span of < 2.8 Myr and 3.7–5.9 Myr, respectively. The study suggests a SN explosion about 5 Myr ago at 30 pc distance. Another study reports an enhancement in the CR intensity dated about 40 kyr ago (Sonett, Morfill, & Jokipii 1987), which is interpreted as the passage across the solar system of the shock wave from a SN exploding about 0.1 Myr ago. Taking into account possible errors of all these estimates, they are consistent and point to a nearby SN explosion some 1 Myr ago (see also discussion in Benítez, Maíz-Apellániz, & Canelles 2002).

It could also be that "fresh" LB contributions from continuous acceleration in the form of shock waves (Bykov & Fleishman 1992), and/or energetic particles coming directly from SNR still influence the spectra and abundances of local CR. The continuous acceleration is connected with the lifetime of a shock wave in the LB. A reasonable estimate is given by the sound crossing time, approximately 2 Myr, for a distance of 200 pc in a 10^6 K plasma (Berghöfer & Breitschwerdt 2002). On the other hand, particle crossing time can be estimated as $t \sim x^2/D \sim 1$ Myr for a typical value of the diffusion coefficient in the ISM $D \sim 10^{28}$ cm s^{-2} and $x \sim 200$ pc. Therefore, the accelerated particles are expected to be present in this region.

3.1. The Calculation Procedure

In our calculations we use the propagation model GALPROP as described elsewhere (Strong & Moskalenko 1998; Moskalenko et al. 2002); for the present purpose the 2D cylindrically symmetrical option is sufficient. For a given halo height z_h the diffusion coefficient

as a function of momentum and the reacceleration or convection parameters is determined by data on secondary-to-primary ratios in CR. The spatial diffusion coefficient is taken as $D_{xx} = \beta D_0 (\rho/\rho_0)^\delta$; the corresponding diffusion in momentum space and other details of the models can be found in our earlier papers.

The injection spectrum nuclei of the Galactic component was taken as a modified power-law in rigidity (Jones et al. 2001), $dq(p)/d\rho \propto \rho^{-\gamma}/\sqrt{1 + (\rho/2)^{-2}}$, for the injected particle density. The proton and He spectra are tuned to the local measurements as described in Moskalenko et al. (2002). The heliospheric modulation is treated using the force-field approximation (Gleeson & Axford 1968).

The Local Bubble spectrum is taken to have the form (as suggested by Bykov & Fleishman 1992, for continous acceleration by interstellar shocks): $df/d\rho \propto \rho^{-\eta} \exp(-\rho/\rho_b)$, where ρ is the rigidity, and ρ_b is the cut off rigidity. ρ_b and the LB source abundances are adjustable parameters. In terms of kinetic energy per nucleon E this can be re-written as

$$\frac{df}{dE} = a(Z, A)\frac{A(E + m)}{Zp}\rho^{-\eta}\exp(-\rho/\rho_b), \tag{1}$$

where $a(Z, A)$ is the abundance of a nucleus (Z, A), Z, A are the nucleus charge and atomic number, correspondingly, m is the atomic mass unit, p is the momentum per nucleon, $\rho_b = \frac{A}{Z}\sqrt{(E_b + m)^2 - m^2}$. The particular spectral shape of the LB component is not important as long as it decreases sharply towards high energies. We show the results obtained with $\eta = 1$, but they are very similar with $\eta = 2$ with ρ_b adjusted correspondingly.

The procedure to tune the CR elemental abundances, secondary/primary nuclei ratios, and antiproton flux we adopted was as follows. The high energy part of B/C ratio and antiproton flux measurements are used to restrict the value of the diffusion coefficient, its energy dependence, and provide a value for the reacceleration level. The Galactic CR elemental source abundances are tuned to the abundances measured at high energies where the heliospheric modulation is weak.

We consider three different models (Table 1) with parameters fixed using the described procedure. They are: the simplest plain diffusion model (PD), and two reacceleration models, which differ by the assumed isotopic abundances in the Galactic CR sources and LB sources. Diffusive reacceleration model I (DR I) has equal isotopic abundances in Galactic CR and LB sources. Diffusive reacceleration model II (DR II) is the same as DR I except that the Local Bubble isotopic abundances are tuned to match the low-energy data by ACE and Ulysses, thus increasing the freedom to fit the data.

The plain diffusion model, without an LB component, has already been discussed in (Moskalenko et al. 2002). It is inconsistent with low energy data on secondary/primary ratios,

and at high energies matching the B/C ratio would cause an overproduction of antiprotons. We do not see a plausible modifications of this model, even including an LB component, which allows to us simultaneously fit antiprotons and the B/C ratio.

Hence we turn to the models with reacceleration. Fig. 1 shows antiproton flux as calculated in the DR I/II models with $\delta = 0.41$ and different normalization constants in the diffusion coefficient, $D_0 = 3.2 \times 10^{28}, 3.8 \times 10^{28}, 4.4 \times 10^{28}$ cm s^{-2} at $\rho = 3$ GV (for antiprotons $\rho = 3$ GV corresponds to kinetic energy ~ 2 GeV). The injection index γ is taken equal to 2.34, and the Alfvén speed $v_A = 25$ km s^{-1}. The antiproton flux at maximum, ~ 2 GeV, appears to be quite sensitive to the value of the diffusion coefficient and allows us to fix it at $D_0 = 3.8 \pm 0.6 \times 10^{28}$ cm s^{-2}. (A 1σ deviation in the data translates to approximately $\pm 15\%$ accuracy in the diffusion coefficient.) The exact value of δ is not essential since we compare with the antiproton measurements at maximum, ~ 2 GeV. The interstellar proton and Helium spectra used are shown in Fig. 2 together with data. It is clear that the error arising from uncertainties in these primary spectra is only $\sim 5\%$.

Further tuning can be done using the high energy part of the B/C ratio, which is not influenced by heliospheric modulation and supposedly contains only a Galactic component of CR. Fig. 3 (left) shows a calculation of the B/C ratio for $E_b = 400$ MV and different energy dependences of the diffusion coefficient. The plotted curves correspond to values of the power-law index $\delta = 0.36, 0.41, 0.46$, while the injection index was tuned to match the high energy spectral data. Index $\delta \sim 0.41$ is chosen as giving the best match.

The B/C ratio as calculated with and without a contribution of the LB component is shown in Fig. 3 (right). The LB component is shown calculated with $\rho_0 = 500, 400, 300$ MeV/nucleon. It is seen, however, that all three provide good agreement with B/C data. By including the LB component, we have therefore been able to obtain a model simultaneously fitting p, He, $\bar{p}$ and B/C data. It now remains to apply this model to the full range of CR isotopes. A summary of our analysis is given in Table 2.

3.2. Fitting all nuclei

The DR I model gives an approximate fit to all elements. Fig. 5 shows three HEAO-3 ranges, 7.5, 10.6, 16.2 GeV/nucleon, combined with ACE 200 MeV/nucleon data. The fit is systematically low[3] at low energies (ACE) by as much as 50% for Co, while the high energy

---

[3]This may be also due to the errors in the production cross sections employed in our calculations or different resolution of instruments, i.e. systematic errors.

data taken separately are consistent within 5–10% (Fig. 5c). Because of this low energy discrepancy we consider further only the model DR II, where we allow GCR and LB source abundances to be different. This model provides best fit to all data at the cost of extra free parameters.

Figs. 5b, 6b, 7b show an average deviation $< \Sigma > = \frac{1}{n} \sum_{i=1}^{n} \frac{A_i^t - A_i^m}{\sigma_i}$, where A_i^t, A_i^m are the calculated and measured abundances for the given energy, and σ_i is the standard deviation.

In DR II model, the Galactic CR source elemental abundances are tuned (at a nominal reference energy of 100 GeV), by a least squares procedure, to the abundances measured by HEAO-3 (Engelmann et al. 1990) at 4.3, 5.6, 7.5, 10.6, 16.2 GeV/nucleon (Figs. 4,6). At these energies the heliospheric modulation is weak (for the epoch 1980 we adopt $\Phi = 800$ MV), and it is in the middle of the logarithmic interval 0.6–35 GeV/nucleon covered by the HEAO-3 measurements and thus the systematic and statistical errors are minimal. Relative isotopic abundances at the source are taken equal to solar system abundances (Anders & Grevesse 1989). The deviations from the data at any particular energy are all within $\sim 5\%$ for $Z < 18$, but become as large a $\sim 10 - 15\%$ for heavier elements, and in case of Co $> 20\%$ (Figs. 6a,c). This gives an idea of possible systematic errors.

The Local Bubble elemental abundances are tuned simultaneously with spectra using the low energy part of the B/C ratio and isotopic abundances at 200 MeV/nucleon from ACE (Wiedenbeck et al. 2001) and Ulysses (DuVernois & Thayer 1996). For many elements ACE and Ulysses abundances differ by 10% (Fig. 7c). For this reason, to the statistical errors shown we added 5% of the systematic error, which is a minimal conservative estimate of the uncertainties in the measurements and modulation potential.

We note that as in the case of other nuclei, there should be an LB contribution to proton and He spectra. The Galactic injection spectra of protons and He should be significantly flatter below several GeV to match the data points at low energies. This does not influence the antiproton production because, (i) the LB does not produce significant amount of secondaries, and (ii) the antiproton threshold production energy is high, ~ 10 GeV.

3.3. Abundances

The DR II model with an LB component shows good overall agreement with data including secondary to primary ratios, spectra, and abundances. Spectra of Boron, Carbon, Oxygen, and iron are shown in Fig. 9 for two modulation levels, 500 and 800 MV.

The derived Galactic CR source abundances and LB source abundances are given in

Table 3 and plotted in Fig. 11. In case of Carbon, the normalization coefficient in the LB component (eq. [1]) is fixed as $a(6, 12) = 7.58 \times 10^{-4}$ cm^{-2} s^{-1} sr^{-1} for $\eta = 1$. The important result is that CR source and LB source abundances of major elements (C, O, Ne, Mg, Si, S, Fe) are in a good agreement.

Abundances of other elements in GCR and LB sources are mostly consistent with each other, and with solar system abundances, within a factor of 2. Abundances of the Si group, Ca, Fe, Ni are near the Solar System abundances. Relative to Silicon, C, N, O, Ne, S are underabundant both in CR source and LB. This agrees with results by other authors where source abundances show a dependence on the ionization potential (or volatility, e.g., Meyer, Drury, & Ellison 1998). Nitrogen in CR sources and LB sources differs by a factor of ~ 3, which may be connected with production cross section errors (see discussion in Appendix A).

Secondary nuclei F, K, Sc, Ti, V appear to be overabundant in the LB sources (shown as upper limits in Fig. 11a). One possible reason for this is the uncertainty in the production cross sections, which is especially large for these nuclei. Sometimes there is no measurement at all; in this case one can use only phenomenological systematics, which are frequently wrong by a factor of two or even more. Often, there is only one measurement at ~ 600 MeV/nucleon, which has to be extrapolated in both directions[4]. This allows only a nearly flat Webber-type or Silberberg-Tsao-type extrapolations while the real cross sections usually have large resonances below several hundred MeV/nucleon, and decrease with energy above a few GeV/nucleon. We note that Davis et al. (2000) used semiempirical cross sections based on Webber, Kish, & Schrier (1990) and also predicted fluxes of sub-Fe elements which are too low.

An estimate of the overall error, which is reflected in derived LB source abundances, can be obtained by assuming the absence of F, K, Sc, Ti, V in the LB source (shown by crosses in Fig. 11). In case of Fluorine, the difference in abundances is negligible. In case of K, Sc, Ti, V, the discrepancy is approximately 20–25%, and can be *removed* by allowing the production cross sections to increase at low energies by 25%, which seems plausible.

Another possibility is errors in flux measurements of the rare CR species. Fig. 12 shows

---

[4]Only the following reactions are well measured, on a sample of natural iron consisting mostly of ^{56}Fe: p+natFe $\rightarrow$ ^{46,47}Sc, ^{48}V, ^{48,51}Cr; we use our fits to these data. Reactions producing other isotopes of Sc, Ti, V on ^{56}Fe, ^{55}Mn, and ^{52}Cr have only one or two measurements. There is no data on the production of Sc, Ti, V on ^{54}Fe, ^{53}Mn, and Cr isotopes (except ^{52}Cr), on production of Sc, Ti, on ^{49}V, and on production of Sc on Ti. These poorly known cross sections contribute to errors on the production of sub-Fe elements at low energies.

the calculated abundances[5] tuned at low energies to the ACE and Ulysses data. Ulysses and ACE measurements are not always in agreement. Note that even for such an abundant nucleus as iron, which is the main contributor to the sub-Fe group, the discrepancy exceeds 10%, while the disagreement in abundance of Sc is $\sim 30\%$.

The derived source overabundance of sub-Fe elements in the LB could also in principle arise from composition differences between the ISM in the LB and solar or Galactic average ISM. This is suggested by the fact that the relative abundances of secondary elements in the LB sources are systematically larger than in the GCR sources (Fig. 11). However, the factors required in case of, e.g., Ti (Ti/Fe = 5% compared to solar or SN 0.1%) appear much larger than could reasonably be expected even for unusual SN types.

Be and B isotopes are assumed all secondary, thus there is no possibility to tune them. The DR II model calculation shows perfect agreement with the data on relative isotopic abundances of Be and B (Fig. 13). This is in contrast with a "standard" reacceleration model, where we obtained a 15% discrepancy with relative abundances of ^{7}Be and ^{9}Be isotopes (Strong & Moskalenko 2001). Other elements are not conclusive because they are present in the sources, but O and Si isotopic distributions still agree very well with data (Webber et al. 1996; Webber, Lukasiak, & McDonald 1997; DuVernois et al. 1996; Hesse et al. 1996; Wiedenbeck et al. 2001) assuming only ^{16}O and ^{28}Si isotopes are present in the LB component.

C and N isotopic distributions do not agree too well, but this may point to a problem with cross sections (see discussion in Appendix A). The calculated ratio ^{13}C/^{12}C ~ 0.11 at 200 MeV/nucleon ($\Phi = 500$ MV) in the model with LB contribution compared to Voyager and Ulysses measurements is still a factor ~ 1.5 too large, which may be connected with overproduction of ^{13}C on ^{15}N.

4. Discussion and Conclusion

In this paper we have considered the possibility that some part of the CR that we measure near the earth consists of a "fresh" component accelerated in the LB. The experimental data (except may be overabundance of Sc, Ti, V) do not contradict this hypothesis. The production cross sections if measured accurately would help to distinguish between different models; as of now, many important channels are not known accurately enough. Such cross section errors lead to errors in important isotopic ratios, which, in turn, are translated into

---

[5]Calculated Li abundance in the plot shows only secondary Lithium produced in CR.

errors in propagation parameters. In our treatment of B and Be production cross sections, as well as some isotopes of other elements, we use all available data and our own fits to them, which should be more accurate than semiempirical systematics by Webber et al. (1990, code version of 1993) and Silberberg, Tsao, & Barghouty (1998, code version of 2000).

We note, that Donato et al. (2001) claim to have obtained agreement with antiproton measurements in a reacceleration plus convection model using the parameters derived from B/C and sub-Fe/Fe ratios (Maurin et al. 2001). Apart from having one more free parameter (convection *plus* reacceleration), they also in fact fitted B/C and sub-Fe/Fe ratios only at HE (since the fitting procedure they employed is simply not sensitive to a few LE points while there are many points to fit at HE). Their calculated ratios at LE are higher than the Voyager and ACE data by approximately 20% or about 6σ (see their Figs. 3,4 in Maurin et al. 2001). This is, however, where the most of the problem lies.

The Local Bubble hypothesis leads to some consequences for radioactive isotopes in CR, which are often used as "radioactive clocks" to determine the Galactic halo size. Be in CR is all secondary (Fig. 12). Therefore, the ratio $^{10}Be/^{9}Be$ is affected only because of changes in the propagation parameters, mainly the diffusion coefficient. The data are still consistent with our adopted halo height of 4 kpc (Fig. 14).

We should also mention that another possibility to get the correct antiproton flux in reacceleration models is to introduce an additional proton component at energies up to approximately 20 GeV. The latter energy is above the antiproton production threshold and effectively produces antiprotons at ~ 2 GeV and below. The intensity and spectral shape of this component could be derived by combining restrictions from antiprotons and diffuse γ-rays. Interestingly this kind of spectrum was used in our HEMN model (hard electrons and modified nucleons, Strong, Moskalenko, & Reimer 2000) to match the spectrum of diffuse γ-rays as observed by EGRET (Hunter et al. 1997). The advantage of this approach is that the diffuse γ-rays which we observe carry information on the large-scale Galactic spectrum of CR (producing $\bar{p}$) while particles we measure may reflect only the local region.

One more (non-standard) interpretation is that the solar modulation is weaker than assumed, and this would eliminate the need for a LB component. With a modulation potential as small as ~ 200 MV one can obtain a consistent reacceleration model combining B/C, antiprotons, and other species simultaneously. The injection spectra in such a model should be flatter at LE to get an agreement with spectral data.

Recently there has appeared some indication that the atmospheric contribution to the antiproton flux measured in the upper atmosphere is underestimated. Monte Carlo simulations of the hadron cascade development in the upper atmosphere have shown that the

antiproton flux induced by pA-reactions on air nuclei is larger, *at least*, by $\sim$30% (Huang, Derome, & Buénerd 2001) compared to often used calculations with analytical production cross sections. This means that the flux of antiprotons in CR in reality may be *lower* by at least 25-30%. If the latter is true, the reacceleration model (even without LB) could still be the best one to describe propagation of nucleon species in the Galaxy.

A. Production cross sections of isotopes of Carbon and Nitrogen

The production cross section of the most abundant ^{12}C isotope is one of the most poorly known. All the data available on its production on ^{16}O and Nitrogen isotopes are summarized in Table 4. The data include also production of ^{12}B, and ^{12}N, which decay to ^{12}C with branching 0.98, and ^{13}O with branching ratio 0.12.

Data on the production of ^{13}C are somewhat more extensive, but some important channels are not measured accurately enough. Most of the data available are summarized in Table 5. The data include also production of ^{13}N, which decays to ^{12}C with branching 1, and ^{13}O with branching 0.88. The production cross section of ^{13}B is very small, fractions of a mb. Fortunately there are data on production of ^{13}N on natural samples of Oxygen and Nitrogen, which contain mostly ^{16}O and ^{14}N isotopes respectively. They probably include also production of ^{13}O, but the cross section must be very small (0.17mb at 2100 MeV/n).

The production cross section of the most abundant ^{14}N isotope is also poorly known. All the data available are summarized in Table 6. The data include also production of ^{14}C, and ^{14}O, which decay to ^{14}N with branching ratio 1.

The main contributor to the production cross section of ^{15}N is ^{16}O (Table 7). The direct and indirect (via ^{15}O) production cross sections are almost equal. The channel $p+^{16}$O $\rightarrow ^{15}$O is well studied since there is a large amount of data on natural sample of Oxygen.

The cumulative (sum over all channels) production cross sections of Carbon and Nitrogen isotopes multiplied by the flux of the corresponding primary isotope in CR at 2 GeV/nucleon are shown in Fig. 15. The main contributor to the production of secondary Carbon and Nitrogen is ^{16}O, accounting for about 80% in case of Nitrogen isotopes. However, in the case of Carbon, the reaction on ^{16}O gives only about 50% with an essential

contribution from Nitrogen isotopes (and ^{13}C in case of ^{12}C).

The contribution of ^{15}N to the production of ^{13}C is especially large (Table 5). This is based on only one experimental point which seems too large compared to the production cross sections on ^{14}N and ^{16}O. This may indicate that the reason for the large fraction of ^{13}C in calculated CR abundances compared to the measurements (see Sections 2 and 3.3) may be errors in the cross sections.

There are more examples of discrepancies in ^{13}C and ^{14}N production cross sections (Tables 5, 6). The cross section of ^{13}C on ^{22}Ne at 580 MeV/nucleon differs significantly from that at 400 MeV/nucleon. The cross section of ^{13}C on ^{26}Mg measured by the same group at 370 and 576 MeV/nucleon differs by a factor of 4 (6.3 mb vs. 25 mb). A similar situation occurs with ^{14}C production on ^{22}Ne at 400, 580, and 894 MeV/nucleon, and on ^{26}Mg at 371 and 576 MeV/nucleon (3.5 mb vs. 9 mb). Fortunately, these latter cross sections do not contribute much to production of ^{13}C and ^{14}N in CR, but these discrepancies indicate the degree of overall uncertainty in the production cross sections.

Cross section errors in production of Carbon may lead to errors in the B/C ratio, which, in turn, are translated into errors on the propagation parameters. Because the CR measurements are now rather accurate, the errors in the cross sections may cause many standard deviations when comparing the model calculations with CR data.

REFERENCES

Alibés, A., Labay, J., & Canal, R. 2001, A&A, submitted, astro-ph/0107016

Alcaraz, J., et al. 2000, Phys. Lett. B, 490, 27

Anders, E., & Grevesse, N. 1989, Geochim. Cosmochim. Acta, 53, 197

Asaoka, Y., et al. 2002, Phys. Rev. Lett., 88, 051101

Benítez, N., Maíz-Apellániz, J., & Canelles, M. 2002, Phys. Rev. Lett., 88, 081101

Berghöfer, T. W., & Breitschwerdt, D. 2002, A&A, 299

Binns, W. R., et al. 1999, Proc. 26th Int. Cosmic Ray Conf. (Salt Lake City), 3, 21

Boezio, M., et al. 1999, ApJ, 518, 457

Boezio, M., et al. 2001, ApJ, 561, 787

Bogomolov, E. A., Lubyanaya, N. D., Romanov, V. A., & Stepanov, S. V., & Shulakova, M. S. 1979, Proc. 16th Int. Cosmic Ray Conf. (Kyoto), 1, 330

Bykov, A. M., & Fleishman, G. D. 1992, MNRAS, 255, 269

Connell, J. J. 1998, ApJ, 501, L59

Connell, J. J. 2001, Proc. 27th Int. Cosmic Ray Conf. (Hamburg), 1751

Davis, A. J., et al. 2000, in AIP Conf. Proc. 528, Acceleration and Transport of Energetic Particles Observed in the Heliosphere (ACE-2000), ed. R. A. Mewaldt et al. (New York: AIP), 421

Davis, A. J., et al. 2001, Proc. 27th Int. Cosmic Ray Conf. (Hamburg), 3971

de Nolfo, G. A., et al. 2001, Proc. 27th Int. Cosmic Ray Conf. (Hamburg), 1659

Donato, F. et al. 2001, ApJ, 563, 172

DuVernois, M. A., Simpson, J. A., & Thayer, M. R. 1996, A&A, 316, 555

DuVernois, M. A., & Thayer, M. R. 1996, ApJ, 465, 982

DuVernois, M. A., Garcia-Munoz, M., Pyle, K. R., Simpson, J. A., & Thayer, M. R. 1996, ApJ, 466, 457

Engelmann, J. J., et al. 1990, A&A, 233, 96

Gleeson, L. J., & Axford, W. I. 1968, ApJ, 154, 1011

Golden, R. L., Horan, S., Mauger, B. G., Badhwar, G. D., Lacy, J. L., Stephens, S. A., Daniel, R. R., & Zipse, J. E. 1979, Phys. Rev. Lett., 43, 1196

Grevesse, N., & Sauval, A. J. 1998, Space Sci. Rev., 85, 161

Hams, T., et al. 2001, Proc. 27th Int. Cosmic Ray Conf. (Hamburg), 1655

Heinz, S., & Sunyaev, R. A. 2002, A&A, in press (astro-ph/0204183)

Hesse A., et al. 1996, A&A, 314, 785

Higdon, J. C., Lingenfelter, R. E., & Ramaty, R. 1998, ApJ, 509, L33

Huang, C. Y., Derome, L., & Buénerd, M. 2001, Proc. 27th Int. Cosmic Ray Conf. (Hamburg), 1707

Hunter, S. D., et al. 1997, ApJ, 481, 205

Jones, F. C., Lukasiak, A., Ptuskin, V., & Webber, W. 2001, Proc. 27th Int. Cosmic Ray Conf. (Hamburg), 1844

Jones, F. C., Lukasiak, A., Ptuskin, V., & Webber, W. 2001, ApJ, 547, 264

Knie, K., Korschinek, G., Faestermann, T., Wallner, C., Scholten, J., & Hillebrandt, W. 1999, Phys. Rev. Lett., 83, 18

Lukasiak, A., Ferrando, P., McDonald, F. B., & Webber, W. R. 1994, ApJ, 426, 366

Lukasiak, A., McDonald, F. B., & Webber, W. R. 1999, Proc. 26th Int. Cosmic Ray Conf. (Salt Lake City), 3, 41

Maiz-Apellaniz, J. 2001, ApJ, 560, L83

Maurin, D., Donato, F., Taillet, R., & Salati, P. 2001, ApJ, 555, 585

Menn, W. et al. 2000, ApJ, 533, 281

Meyer, J.-P., Drury, L. O'C., & Ellison, D. C. 1998, Space Sci. Rev., 86, 179

Mitchell, J. W., et al. 1996, Phys. Rev. Lett., 76, 3057

Molnar, A., & Simon, M. 2001, Proc. 27th Int. Cosmic Ray Conf. (Hamburg), 1877

Morfill, G. E., & Freyberg, M. J. 1998, in Lecture Notes in Physics 506, The Local Bubble and Beyond, Proc. IAU Colluquium No. 166, ed. by D. Breitschwerdt et al. (Berlin: Springer), 177

Moskalenko, I. V., Mashnik, S. G., & Strong, A. W. 2001a, Proc. 27th Int. Cosmic Ray Conf. (Hamburg), 1836

Moskalenko, I. V., Strong, A. W., Ormes, J. F., Potgieter, M. S., & Langner, U. W. 2001b, Proc. 27th Int. Cosmic Ray Conf. (Hamburg), 1868

Moskalenko, I. V., Strong, A. W., Ormes, J. F., & Potgieter, M. S. 2002, ApJ, 565, 280

Orito, S., et al. 2000, Phys. Rev. Lett., 84, 1078

Sanuki, T., et al. 2000, ApJ, 545, 1135

Sfeir, D. M., Lallement, R., Crifo, F., & Welsh, B. Y. 1999, A&A, 346, 785

Silberberg, R., Tsao, C. H., & Barghouty, A. F. 1998, ApJ, 501, 911

Sina, R., Ptuskin, V. S., & Seo, E. S. 2001, Proc. 27th Int. Cosmic Ray Conf. (Hamburg), 1873

Sofia, U. J., & Meyer, D. M. 2001, ApJ, 554, L221

Sonett, C. P., Morfill, G. E., & Jokipii, J. R. 1987, Nature, 330, 458

Stephens, S. A., & Streitmatter, R. A. 1998, ApJ, 505, 266

Stochaj, S. J., et al. 2001, ApJ, in press

Strong, A. W., & Moskalenko, I. V. 1998, ApJ, 509, 212

Strong, A. W., & Moskalenko, I. V. 2001, Adv. Space Res., 27, 717

Strong, A. W., Moskalenko, I. V., & Reimer, O. 2000, ApJ, 537, 763; Erratum: 2000, ApJ, 541, 1109

Webber, W. R., Kish, J. C., & Schrier, D. A. 1990, Phys. Rev. C, 41, 566

Webber, W. R., Lukasiak, A., McDonald, F. B., & Ferrando, P., 1996, ApJ, 457, 435

Webber, W. R., Lukasiak, A., & McDonald, F. B., 1996, ApJ, 476, 766

Wiedenbeck, M. E., et al. 2001, Space Sci. Rev., 99, 15

Woosley, S. E., & Weaver, T. A. 1995, ApJS, 101, 181

Table 1.   Propagation parameter sets.

| Model | Injection index, γ | Diffusion coefficient[a] | | Alfvén speed,[b] $v_A/\sqrt{w}$, km s^{-1} | Source abundances |
		D_0, cm^2 s^{-1}	Index, δ		
Plain Diffusion (PD)	2.16	3.10×10^{28}	0.60	—	—
Diffusive Reacceleration I (DR I)	2.34	3.80×10^{28}	0.41	25	LBS=CRS
Diffusive Reacceleration II (DR II)	2.34	3.80×10^{28}	0.41	25	LBS$\neq$CRS

Note. — Adopted halo size $z_h = 4$ kpc.

[a]$\rho_0 = 3$ GV, index δ is shown below/above ρ_0.

[b]v_A is the Alfvén speed, and w is defined as the ratio of MHD wave energy density to magnetic field energy density.

Table 2.   Summary of model predictions.

| Model | B/C | Antiprotons | Source abundances | |
			Major elements	Secondary elements
PD	Too large at low energies	Fair	Good	Bad at low energies
DR I	Good	Good	Good	Discrepancy: low vs. high energies
DR II	Good	Good	Good	Good

Table 3.   Elemental abundances[a]

Z	Solar System	LB Sources	Galactic Sources
6	9.324	4.083	4.025
7	2.344	7.667×10^{-1}	2.961×10^{-1}
8	19.04	6.300	5.239
9	8.901×10^{-4}	$1.167 \times 10^{-2}*$	1.431×10^{-4}
10	3.380	6.833×10^{-1}	6.126×10^{-1}
11	6.028×10^{-2}	1.050×10^{-1}	3.506×10^{-2}
12	1.070	1.400	1.059
13	8.310×10^{-2}	1.633×10^{-1}	8.014×10^{-2}
14	1.	1.	1.
15	7.944×10^{-3}	8.333×10^{-3}	9.445×10^{-3}
16	6.028×10^{-1}	1.083×10^{-1}	1.377×10^{-1}
17	8.901×10^{-3}	6.667×10^{-3}	3.377×10^{-3}
18	7.070×10^{-2}	3.667×10^{-2}	1.757×10^{-2}
19	3.718×10^{-3}	$2.500 \times 10^{-2}*$	5.009×10^{-3}
20	6.451×10^{-2}	8.333×10^{-2}	5.695×10^{-2}
21	4.169×10^{-5}	$1.333 \times 10^{-2}*$	0.
22	2.958×10^{-3}	$5.667 \times 10^{-2}*$	2.147×10^{-3}
23	2.817×10^{-4}	$2.167 \times 10^{-2}*$	8.586×10^{-4}
24	1.318×10^{-2}	5.500×10^{-2}	2.697×10^{-2}
25	6.901×10^{-3}	1.667×10^{-2}	2.261×10^{-2}
26	8.901×10^{-1}	7.617×10^{-1}	9.777×10^{-1}
27	2.344×10^{-3}	4.333×10^{-3}	1.860×10^{-3}
28	5.014×10^{-2}	3.417×10^{-2}	5.695×10^{-2}

[a]Normalized to Si=1.

*Upper limit.

Table 4. Collection of ^{12}C production cross section data.

Primary Nucleus	Secondary Nucleus	Energy, MeV/nucleus	Cross section, mbarn	Error, mbarn	Reference
^{14}N	^{12}C	377	56.90	-0.040	! [We98]
^{14}N	—	600	52.10	0.781	! [105.]
^{15}N	—	373	30.00	-0.040	! [We98]
^{16}O	—	389	33.90	-0.040	! [We98]
^{16}O	—	600	33.60	0.504	! [105.]
^{16}O	—	2100	32.30	4.800	! [Ol83]
^{16}O	^{12}B	600	1.10	0.110	! [105.]
^{16}O	—	2100	1.45	0.170	! [Ol83]
^{14}N	^{12}N	600	1.10	0.110	! [105.]
^{16}O	—	600	0.30	0.030	! [105.]
^{16}O	—	2100	0.40	0.070	! [Ol83]

Table 5. Collection of ^{13}C production cross section data.

Primary Nucleus	Secondary Nucleus	Energy, MeV/nucleus	Cross section, mbarn	Error, mbarn	Reference
^{14}N	^{13}C	377	7.60	-0.040	! [We98]
^{14}N	—	600	9.60	0.144	! [105.]
^{14}N	—	500	8.60	-0.200	! [We98prc]
^{15}N	—	373	*35.30*	-0.040	! [We98]
^{16}O	—	389	17.40	-0.040	! [We98]
^{16}O	—	600	18.00	0.270	! [105.]
^{16}O	—	2100	17.80	1.700	! [Ol83]
^{20}Ne	—	414	15.30	-0.040	! [We98]
^{20}Ne	—	600	15.70	0.236	! [105.]
^{22}Ne	—	377	17.80	1.400	! [108.]
^{22}Ne	—	401	*15.30*	-0.040	! [We98]
^{22}Ne	—	581	*21.90*	1.900	! [108.]
^{22}Ne	—	894	19.00	1.600	! [108.]
^{26}Mg	—	371	*6.30*	1.200	! [108.]
^{26}Mg	—	576	*25.00*	2.800	! [108.]
^{14}N	^{13}N	377	7.40	-0.080	! [We98]
^{14}N	—	500	7.50	-0.200	! [We98prc]
^{14}N	—	600	7.50	0.225	! [105.]
^{15}N	—	373	4.30	-0.260	! [We98]
^{15}N	—	500	4.30	-0.200	! [We98prc]
^{16}O	—	389	4.60	-0.160	! [We98]
^{16}O	—	600	5.70	0.285	! [105.]
^{16}O	—	2100	4.49	0.460	! [Ol83]
^{20}Ne	—	414	5.10	-0.160	! [We98]
^{20}Ne	—	600	4.10	0.205	! [105.]
^{22}Ne	—	377	0.50	0.100	! [108.]
^{22}Ne	—	401	1.60	-0.160	! [We98]
^{22}Ne	—	581	0.50	0.100	! [108.]
^{22}Ne	—	894	0.70	0.200	! [108.]
^{24}Mg	—	600	6.00	0.300	! [105.]
^{26}Mg	—	371	0.30	0.100	! [108.]
^{26}Mg	—	576	0.10	0.100	! [108.]

Table 6.   Collection of ^{14}N production cross section data.

Primary Nucleus	Secondary Nucleus	Energy, MeV/nucleus	Cross section, mbarn	Error, mbarn	Reference
^{15}N	^{14}N	373	27.60	-0.100	! [We98]*
^{15}N	—	500	29.60	-0.100	! [We98prc]
^{16}O	—	389	31.10	-0.040	! [We98]
^{16}O	—	600	31.00	0.465	! [105.]
^{16}O	—	2100	31.00	3.300	! [Ol83]
^{15}N	^{14}C	373	10.30	-0.040	! [We98]
^{15}N	—	500	10.30	-0.100	! [We98prc]
^{16}O	—	389	1.70	-0.080	! [We98]
^{16}O	—	500	1.70	-0.200	! [We98prc]
^{16}O	—	600	1.70	0.085	! [105.]
^{16}O	—	2100	3.69	0.380	! [Ol83]
^{20}Ne	—	414	2.20	-0.080	! [We98]
^{20}Ne	—	600	2.30	0.115	! [105.]
^{22}Ne	—	377	8.10	0.700	! [108.]
^{22}Ne	—	401	*7.70*	-0.040	! [We98]
^{22}Ne	—	581	*10.20*	1.200	! [108.]
^{22}Ne	—	894	*8.60*	0.900	! [108.]
^{26}Mg	—	371	*3.50*	0.700	! [108.]
^{26}Mg	—	576	*9.00*	1.300	! [108.]
^{16}O	^{14}O	389	1.30	-0.260	! [We98]
^{16}O	—	500	1.30	-0.200	! [We98prc]
^{16}O	—	600	1.20	0.120	! [105.]
^{16}O	—	2100	0.75	0.120	! [Ol83]
^{20}Ne	—	600	1.00	0.100	! [105.]
^{24}Mg	—	600	1.50	0.150	! [105.]

Table 7. Collection of ^{15}N production cross section data.

Primary Nucleus	Secondary Nucleus	Energy, MeV/nucleus	Cross section, mbarn	Error, mbarn	Reference
^{16}O	^{15}N	389	33.60	-0.040	! [We98]
^{16}O	—	500	34.30	-0.100	! [We98prc]
^{16}O	—	600	34.90	0.524	! [105.]
^{16}O	—	2100	34.30	3.300	! [Ol83]
^{20}Ne	—	414	24.00	-0.040	! [We98]
^{20}Ne	—	600	27.80	0.417	! [105.]
^{22}Ne	—	377	36.20	2.100	! [108.]
^{22}Ne	—	401	32.90	-0.040	! [We98]
^{22}Ne	—	581	39.00	2.500	! [108.]
^{22}Ne	—	894	33.50	2.100	! [108.]
^{24}Mg	—	600	14.00	0.420	! [105.]
^{26}Mg	—	371	19.70	2.100	! [108.]
^{26}Mg	—	576	29.90	3.000	! [108.]
^{22}Ne	^{15}C	377	0.70	0.200	! [108.]
^{22}Ne	—	581	0.80	0.200	! [108.]
^{22}Ne	—	894	0.60	0.100	! [108.]
^{26}Mg	—	371	0.90	0.300	! [108.]
^{26}Mg	—	576	0.40	0.300	! [108.]
^{16}O	^{15}O	389	30.70	-0.040	! [We98]
^{16}O	—	500	30.50	-0.100	! [We98prc]
^{16}O	—	600	30.30	0.455	! [105.]
^{16}O	—	2100	27.30	2.600	! [Ol83]
^{20}Ne	—	414	14.90	-0.080	! [We98]
^{20}Ne	—	600	16.20	0.486	! [105.]
^{21}Ne	—	600	7.80	-0.260	! [We98prc]
^{22}Ne	—	377	2.00	0.300	! [108.]
^{22}Ne	—	401	1.60	-0.160	! [We98]
^{22}Ne	—	581	1.60	0.300	! [108.]
^{22}Ne	—	894	2.80	0.400	! [108.]
^{22}Na	—	600	10.90	-0.260	! [We98prc]
^{23}Na	—	600	11.10	-0.260	! [We98prc]
^{24}Mg	—	600	8.60	0.258	! [105.]
^{25}Mg	—	600	6.00	-0.260	! [We98prc]
^{26}Mg	—	371	1.10	0.300	! [108.]
^{26}Mg	—	576	0.20	0.200	! [108.]
^{26}Al	—	600	4.10	-0.260	! [We98prc]
^{27}Al	—	600	7.10	-0.180	! [We98prc]

Table 7—Continued

Primary Nucleus	Secondary Nucleus	Energy, MeV/nucleus	Cross section, mbarn	Error, mbarn	Reference
^{28}Si	—	600	5.60	-0.100	! [We98prc]
^{29}Si	—	600	2.40	-0.260	! [We98prc]
^{32}S	—	365	1.30	0.500	! [111.]
^{32}S	—	571	3.60	0.700	! [111.]
^{32}S	—	770	4.60	1.000	! [111.]

Figures
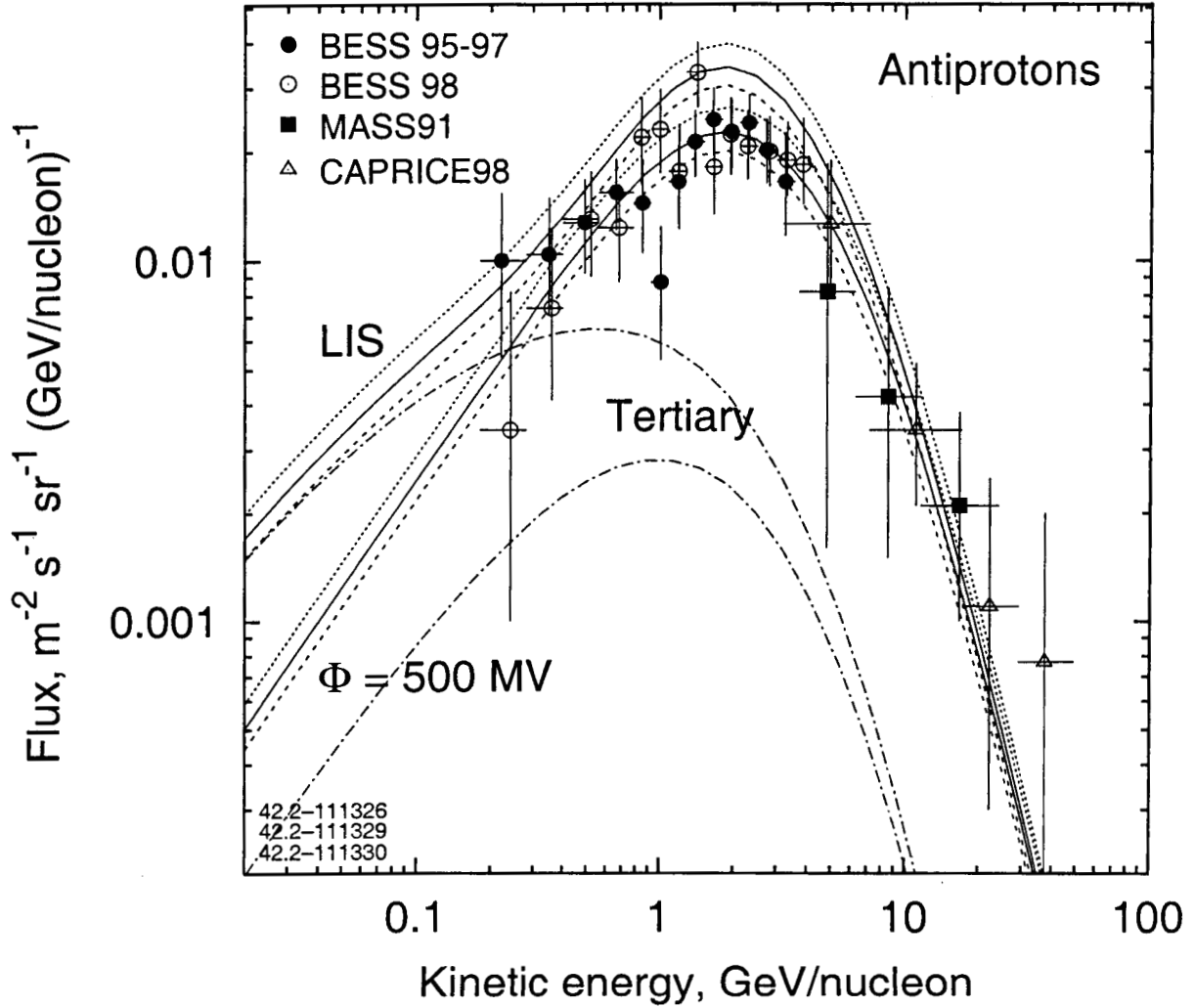
Fig. 1.— Antiproton flux calculated in DR I/II models with different normalization values, D_0 cm s^{-2}, in the diffusion coefficient $D_0 = 3.2 \times 10^{28}$ (dots), 3.8×10^{28} (solid), 4.4×10^{28} (dashes), at $\rho_0 = 3$ GV, and $\delta = 0.41$. Upper curves – interstellar (LIS), modulation was made with $\Phi = 500$ MV (force field, lower curves). Data: BESS 95-97 (Orito et al. 2000), BESS 98 (Asaoka et al. 2002) MASS91 (Stochaj et al. 2001), CAPRICE98 (Boezio et al. 2001). The top curves are the total secondary $\bar{p}$'s. The two lowest curves (dash-dot) marked "tertiary" show separately the LIS spectrum and modulated "tertiary" component for $D_0 = 3.8 \times 10^{28}$ cm s^{-2}.
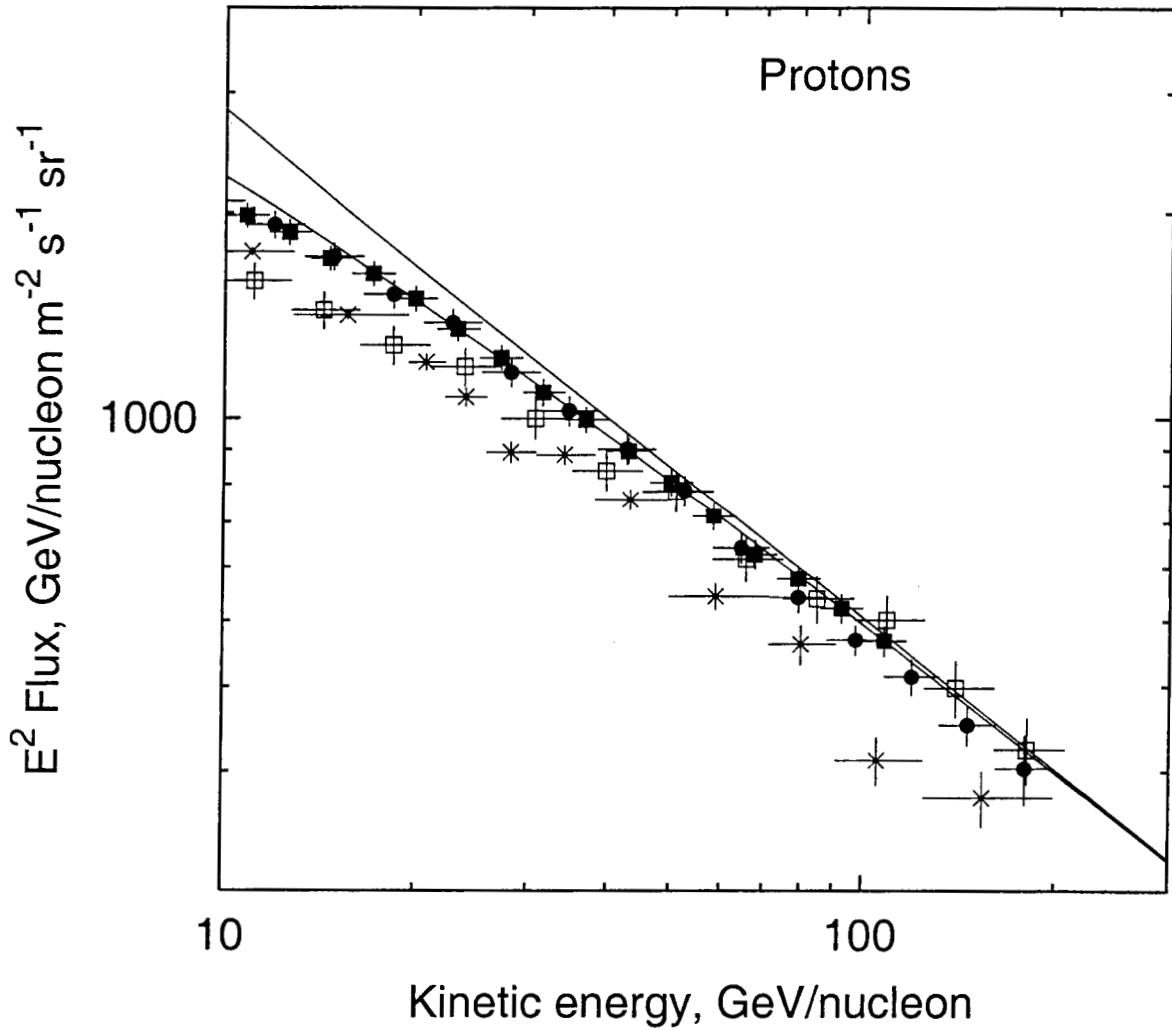
Fig. 2.— The proton spectrum as calculated in models DR I/II compared with the data (upper curve - LIS, lower - modulated to 500 MV). Data: IMAX (Menn et al. 2000), CAPRICE (Boezio et al. 1999), BESS (Sanuki et al. 2000), AMS (Alcaraz et al. 2000).
renormalize the proton flux in the galdef-file
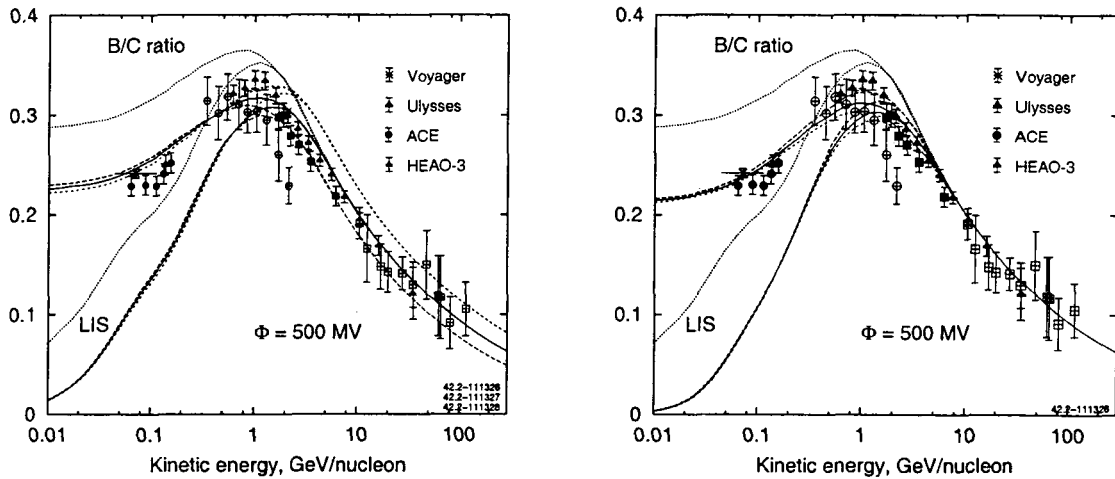
Fig. 3.— *Left:* B/C ratio calculated without (dots) and with (solid, dashes) LB contribution, $E_b = 300$ MeV/nucleon, with different energy dependence in the diffusion coefficient, $\delta = 0.36$ (dashes), 0.41 (solid), 0.46 (short dashes). Lower curves – interstellar (LIS), upper – modulated (force field, $\Phi = 500$ MV). Data below 200 MeV/nucleon: ACE (Davis et al. 2000), Ulysses (DuVernois, Simpson, & Thayer 1996), Voyager (Lukasiak, McDonald, & Webber 1999); high energy data: HEAO-3 (Engelmann et al. 1990), for other references see Stephens & Streitmatter (1998). *Right:* B/C ratio calculated without LB contribution (dotted), and with $E_b = 500$ (long dash), 400 (solid), 300 MeV/nucleon (short dash). Lower curves LIS, upper modulated (force field, $\Phi = 500$ MV). Data as in Fig. 3 (left).
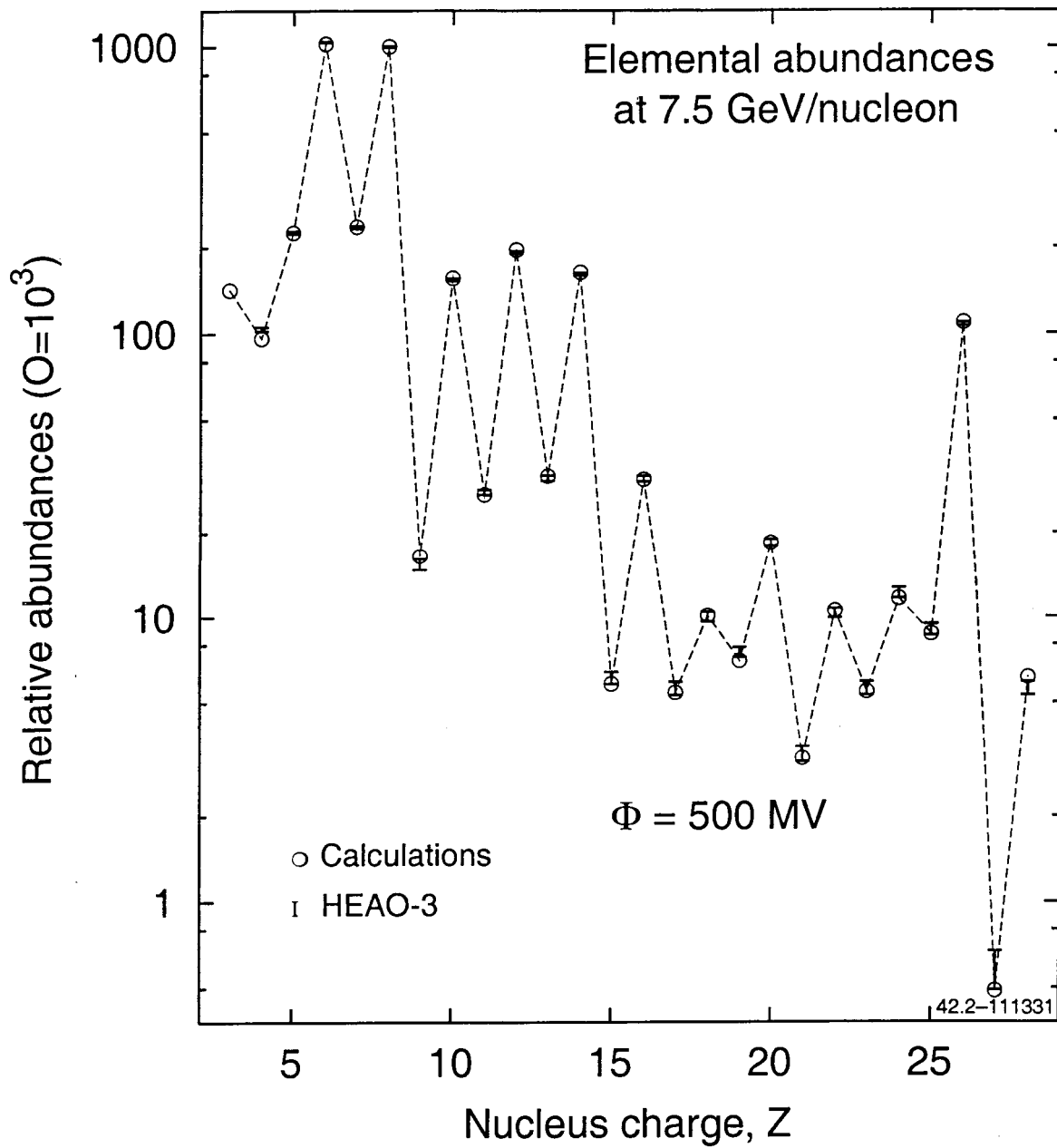
Fig. 4.— Calculated propagated elemental abundances at 7.5 GeV/nucleon. Modulation - force field, $\Phi = 500$ MV. Data: HEAO-3 (Engelmann et al. 1990).

HE vs. LE Abundances -- DR I
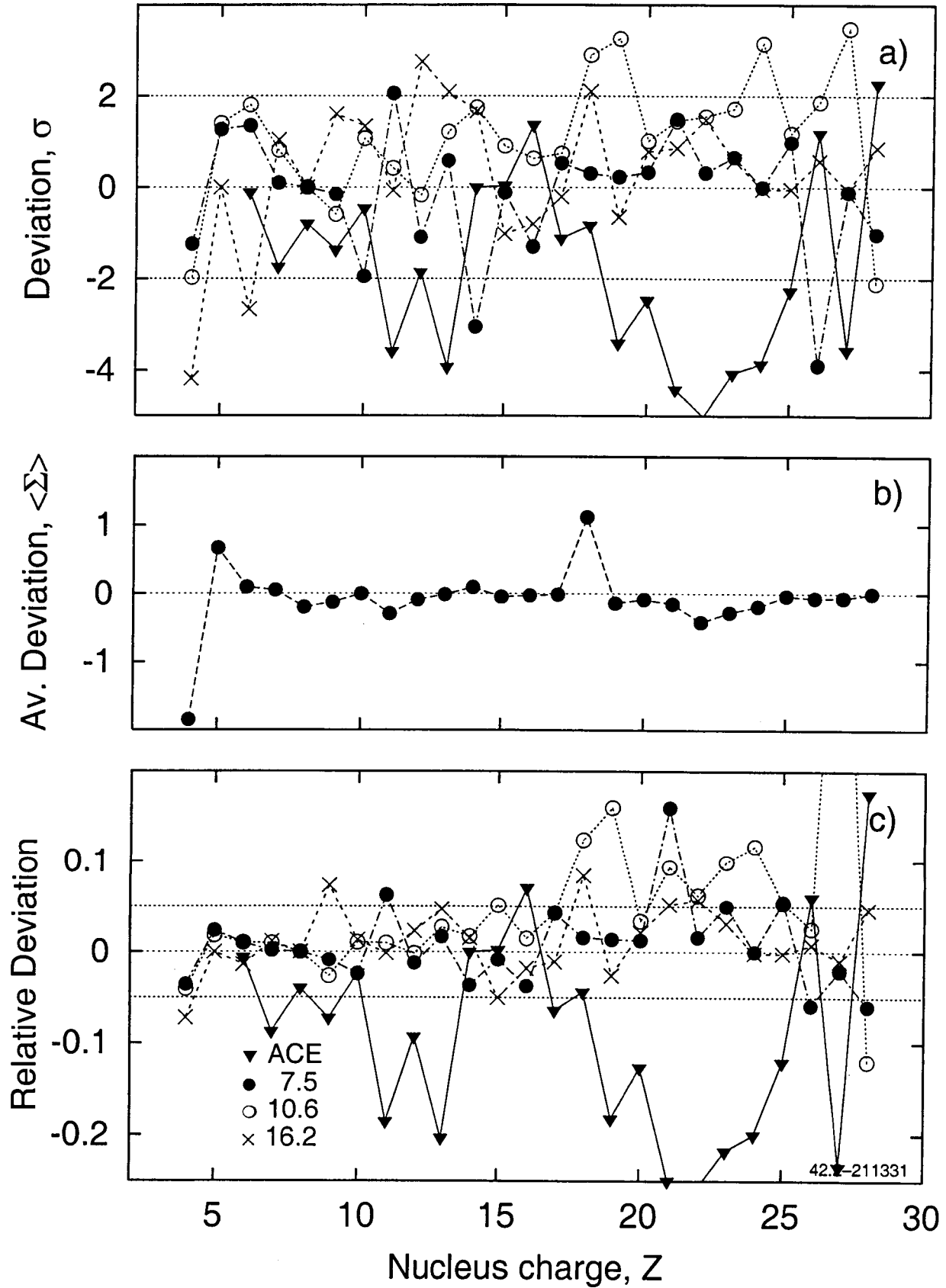
Fig. 5.— Deviation of propagated abundances (model DR I) from measured by HEAO-3 at 7.5, 10.6, 16.2 GeV/nucleon (Engelmann et al. 1990) and ACE at 200 MeV/nucleon (Wiedenbeck et al. 2001) taken together. (a) separately for each energy in σ's, (b) averaged for four energies in σ's, and (c) relative. **tune later**

HE Abundances -- DR II
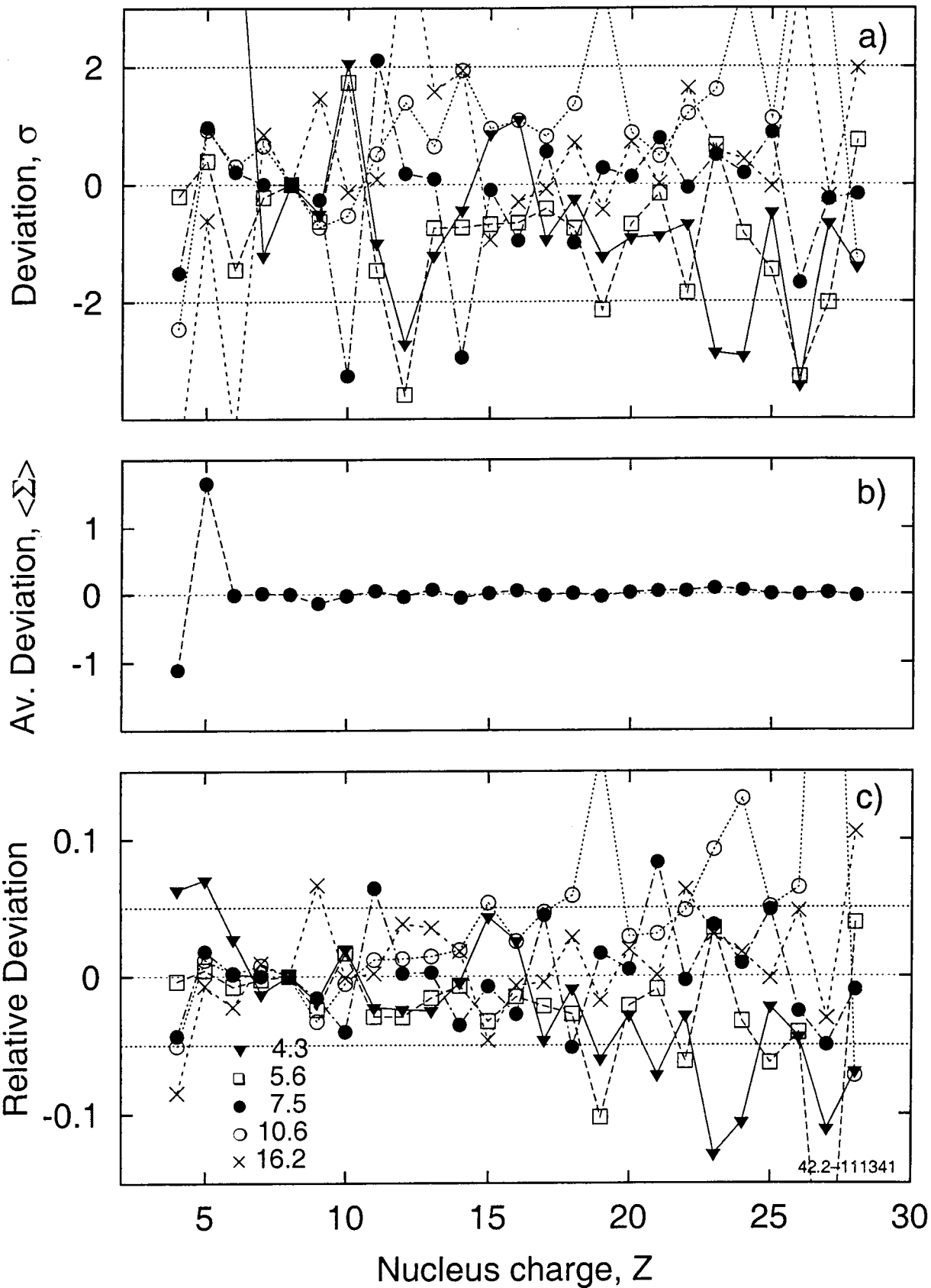
Fig. 6.— Deviation of propagated abundances (model DR II) from measured ones at 4.3, 5.6, 7.5, 10.6, 16.2 GeV/nucleon (HEAO-3, Engelmann et al. 1990) given (a) separately for each energy in σ's, (b) averaged for all five energies in σ's, and (c) relative.

LE Abundances -- DR II
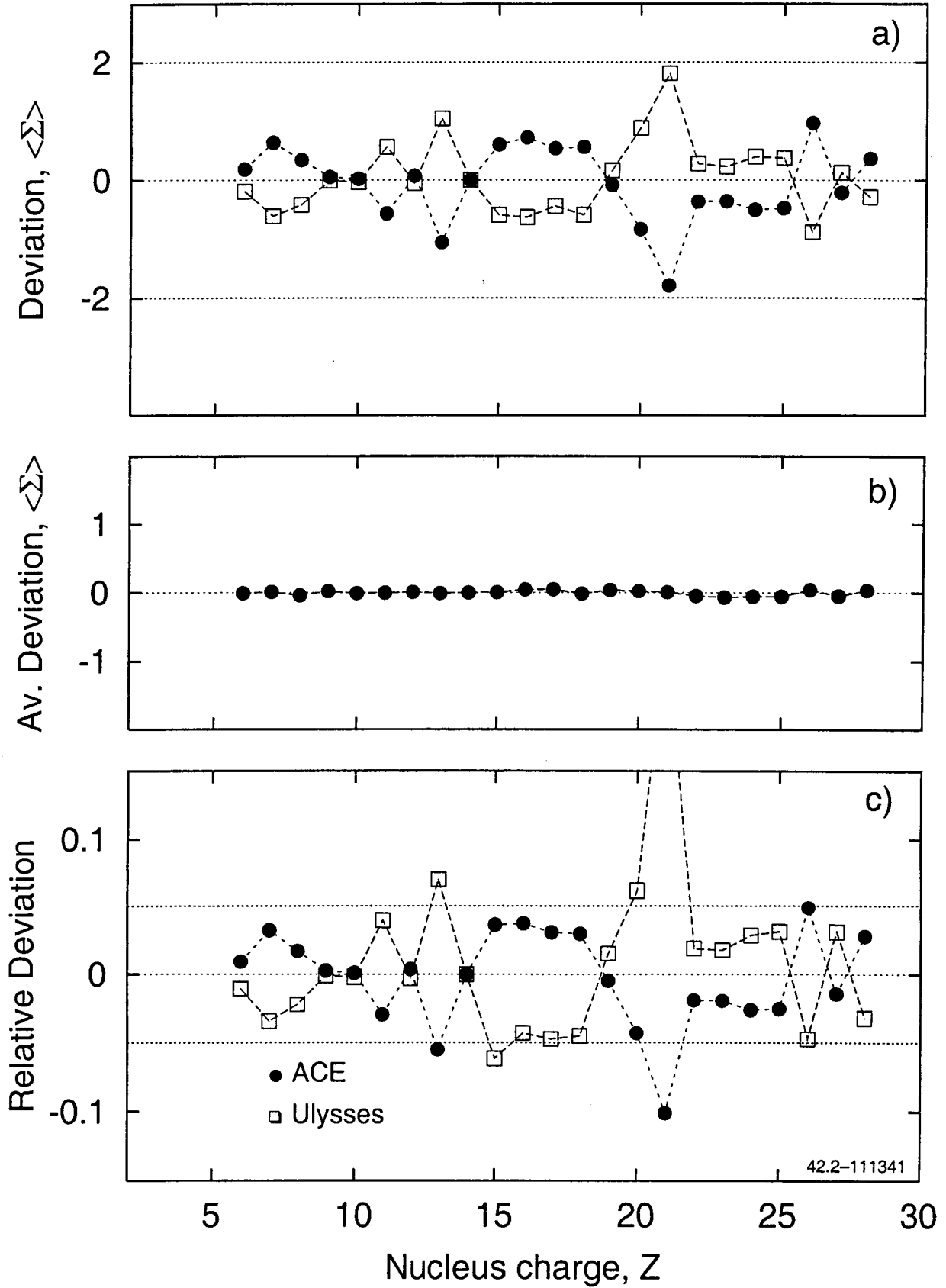
Fig. 7.— Deviation of propagated abundances (model DR II) from measured by ACE (Wiedenbeck et al. 2001) and Ulysses (DuVernois & Thayer 1996) given (a) separately for each energy in σ's, (b) averaged for both sets of data in σ's, and (c) relative.
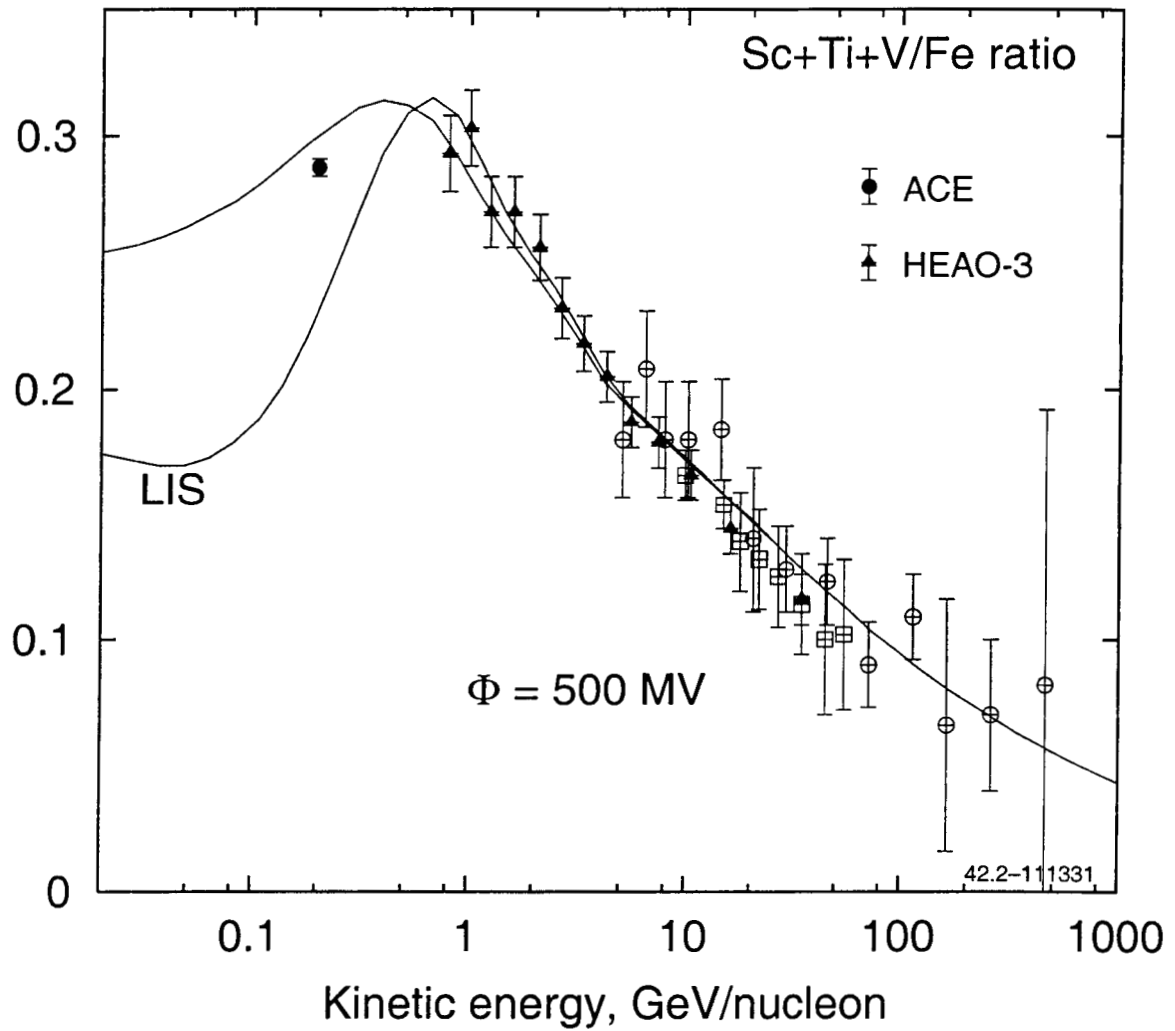
Fig. 8.— Sub-Fe/Fe ratio calculated with LB contribution, and with $\rho_0 = 400$ MeV/nucleon. Lower curves LIS, upper modulated (force field, $\Phi = 500$ MV). Data: ACE (Wiedenbeck et al. 2001), HEAO-3 (Engelmann et al. 1990), for other references see Stephens & Streitmatter (1998).
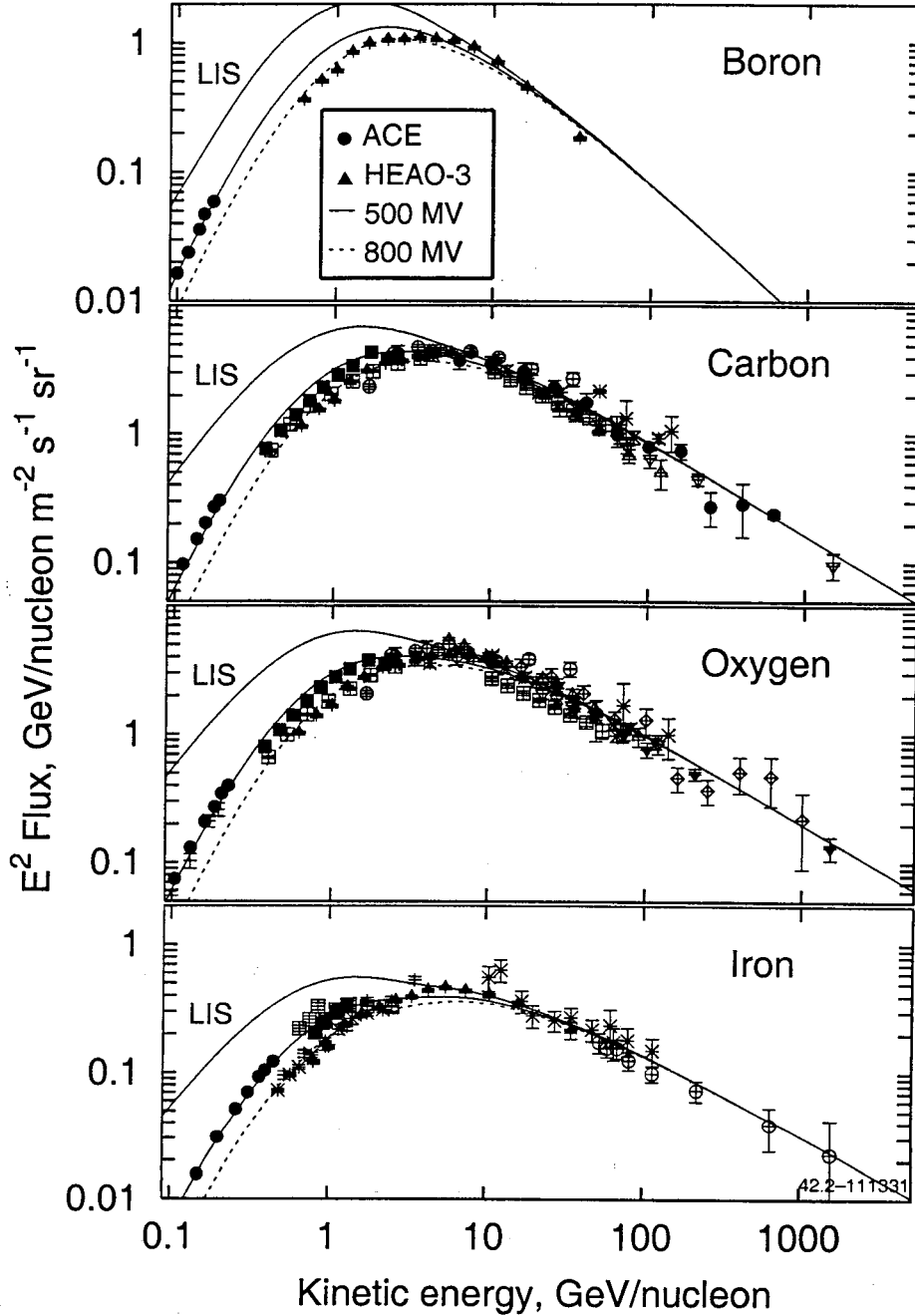
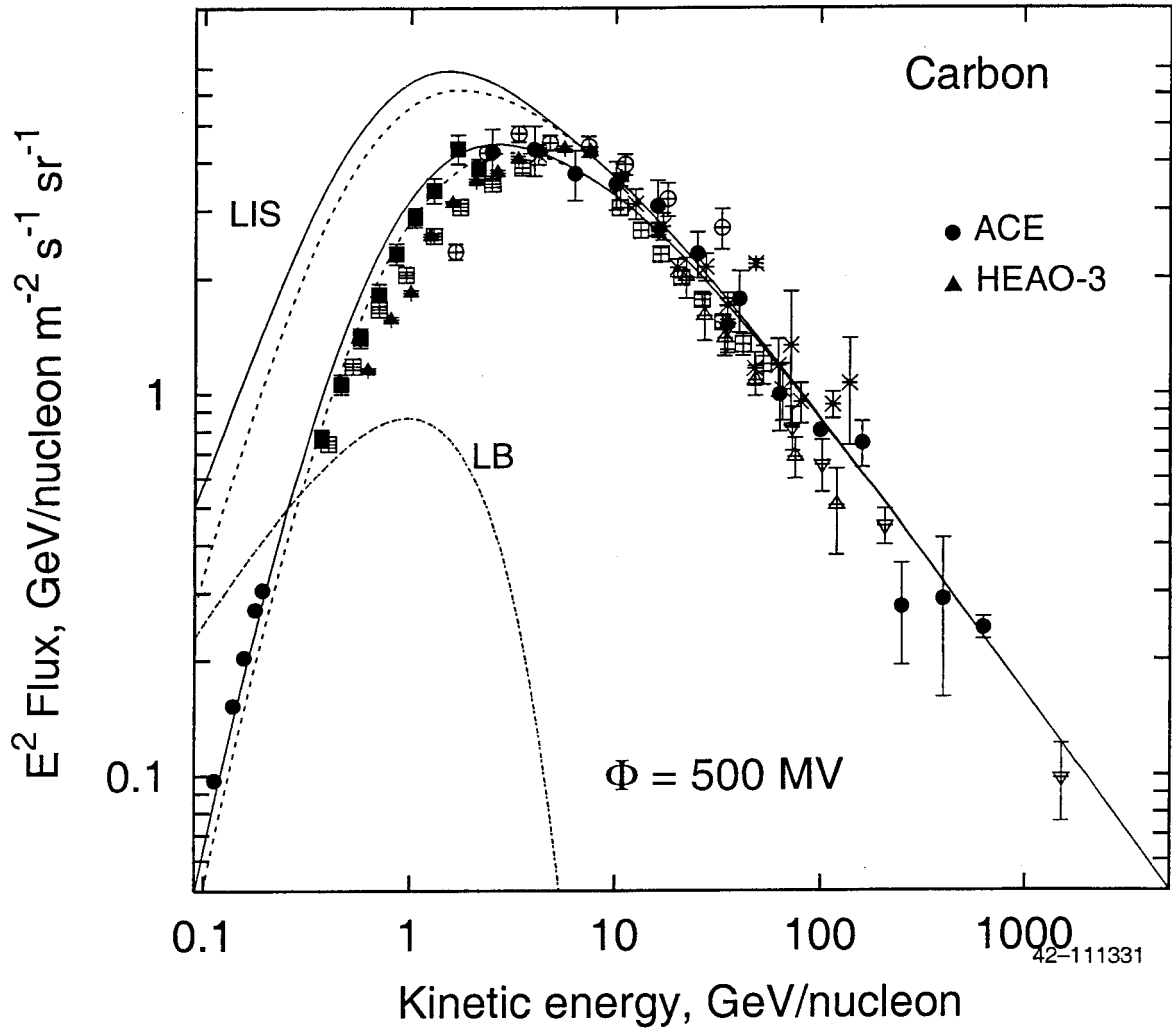Fig. 9.— Spectra of Boron, Carbon, Oxygen, and iron (from top to bottom) calculated with LB contribution. Upper curves - LIS, lower curves – modulated using force field approximation ($\Phi = 500$ MV – solid curves, $\Phi = 800$ MV – dashes). Data: ACE (Davis et al. 2000, 2001), HEAO-3 (Engelmann et al. 1990), for other references see Stephens & Streitmatter (1998).

Fig. 10.— Spectrum of Carbon calculated with (solid) and without (dashes) LB contribution. Upper curves - LIS, lower curves modulated using force field approximation ($\Phi = 500$ MV). Local Bubble (LB) interstellar spectrum is shown by dots. Data as in Fig. 9.
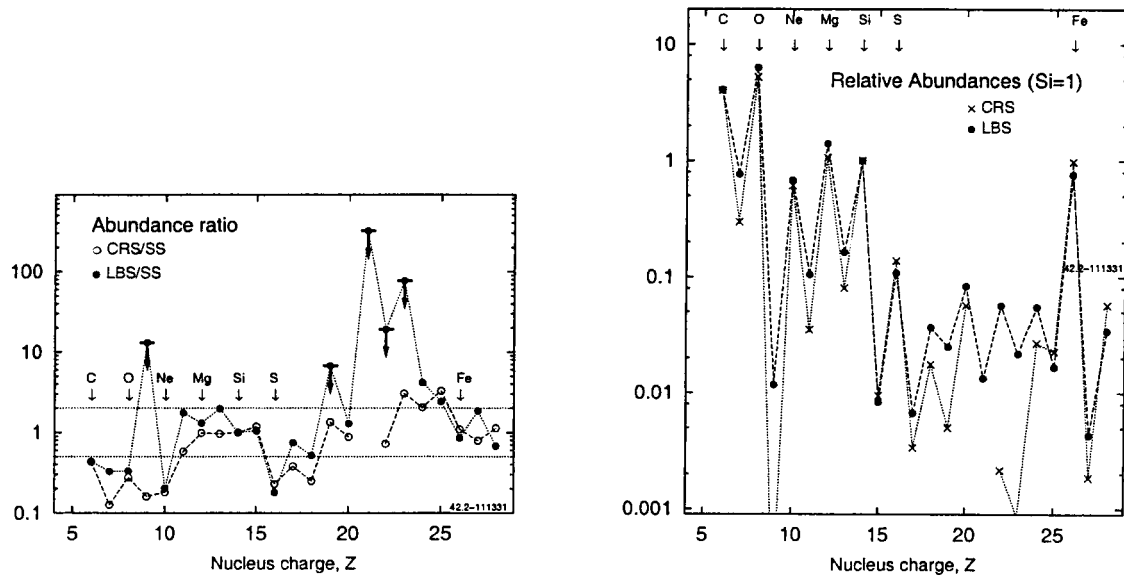
Fig. 11.— *Left:* Derived abundance ratios CR-source/Solar-System (CRS/SS) and LB-source/Solar-System (LBS/SS), normalized to Silicon. Relative abundances for F, K, Sc, Ti, V are shown as upper limits. Solar system abundances from Grevesse & Sauval (1998). The dotted lines plotted at 1/2 and 2. *Right:* Derived CR source and LB source abundances normalized to Silicon.
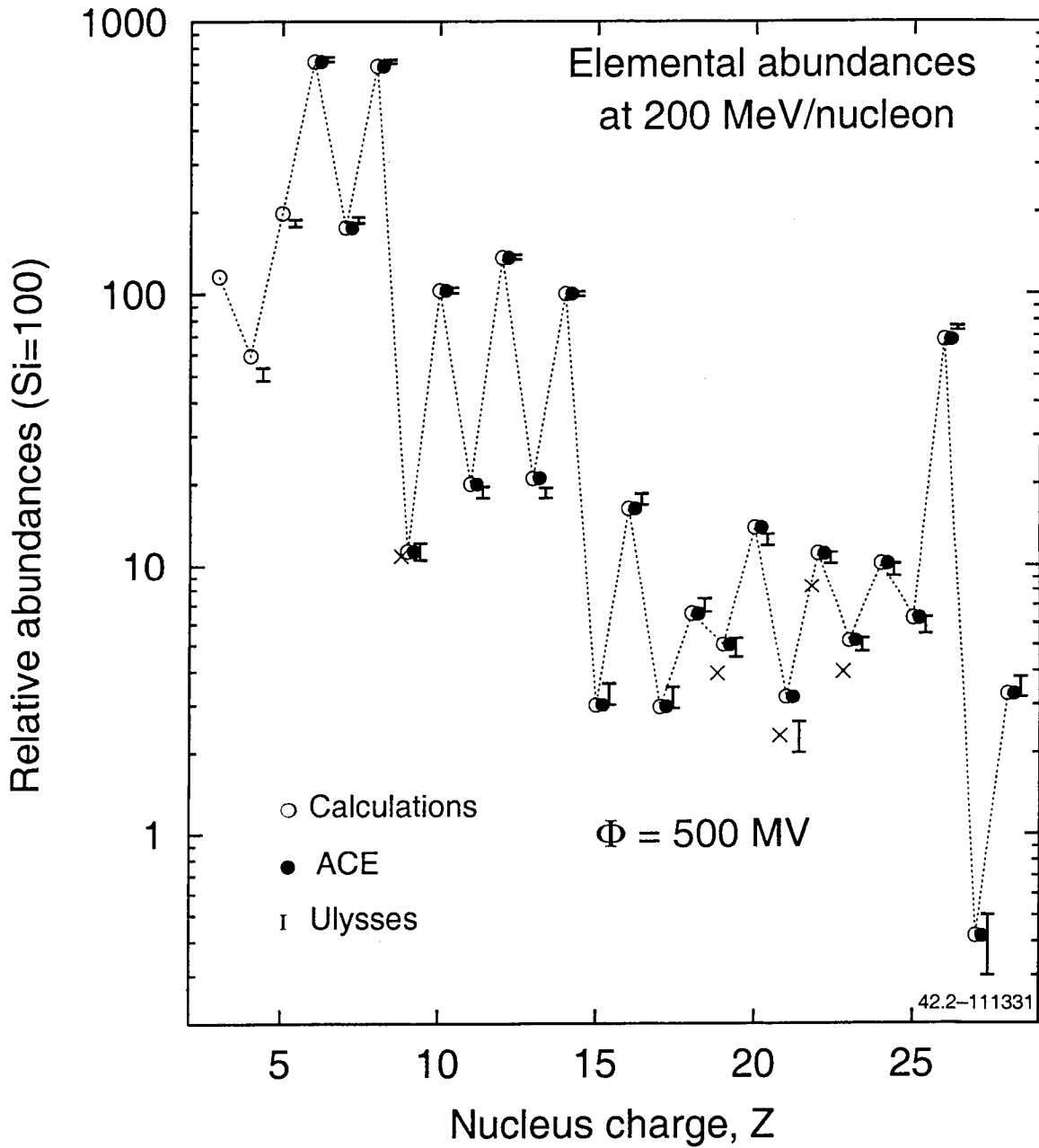
Fig. 12.— Propagated elemental abundances at 200 MeV/nucleon with LB contribution. Crosses show the calculated abundances assuming no F, K, Sc, Ti, V in the LB source. Data: ACE (Wiedenbeck et al. 2001), Ulysses (DuVernois & Thayer 1996).
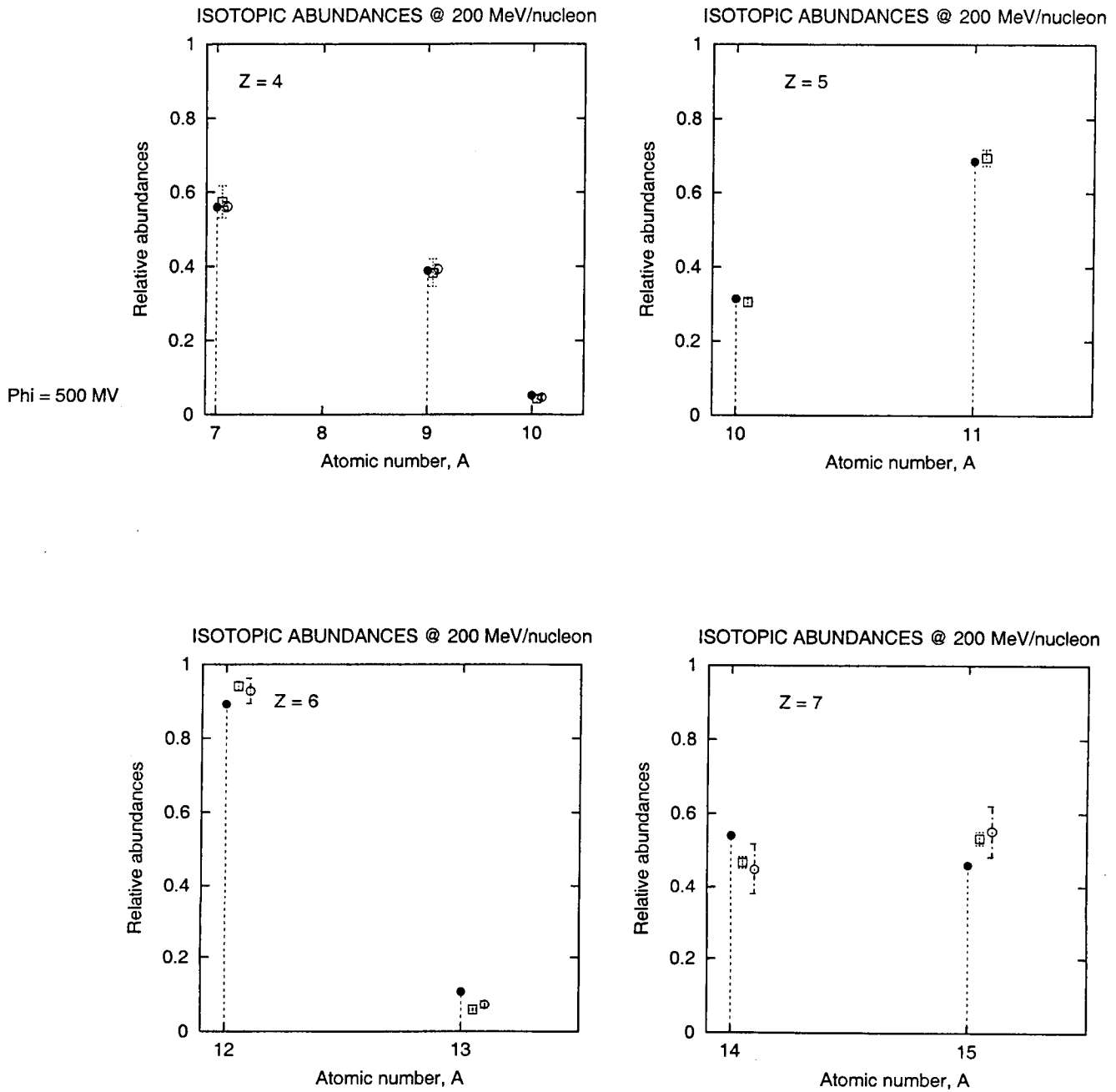
ISOTOPIC ABUNDANCES @ 200 MeV/nucleon

ISOTOPIC ABUNDANCES @ 200 MeV/nucleon

ISOTOPIC ABUNDANCES @ 200 MeV/nucleon

ISOTOPIC ABUNDANCES @ 200 MeV/nucleon

Fig. 13.— Be, B, C, and N isotope distribution as calculated in DR II model compare to the data. Data: Be: Ulysses (Connell 1998), Voyager (Lukasiak et al. 1999), B: Voyager (Lukasiak et al. 1999), C,N: Voyager (Webber et al. 1996), Ulysses (DuVernois et al. 1996).
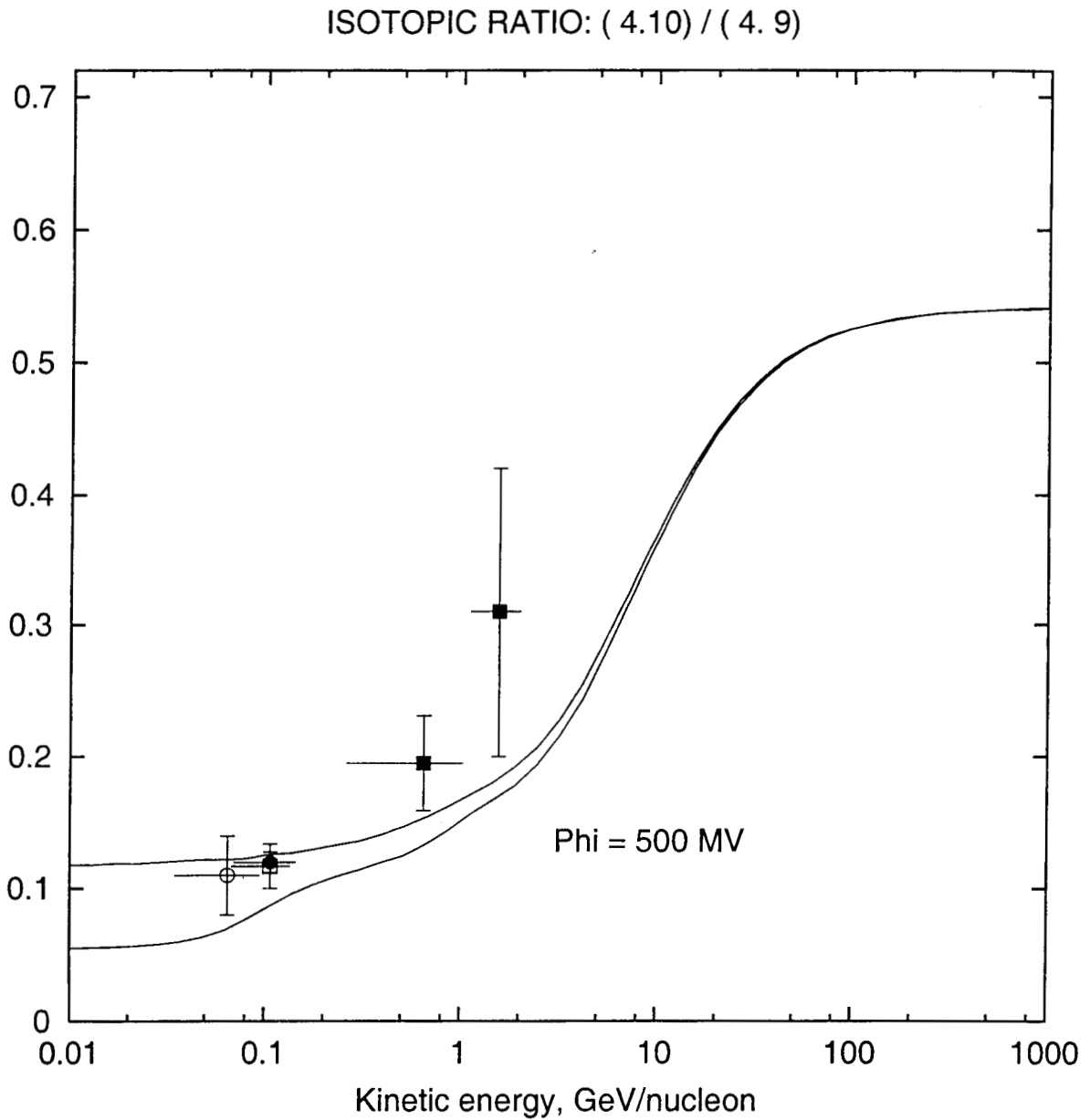
ISOTOPIC RATIO: (4.10) / (4. 9)

Fig. 14.— ^{10}Be/^{9}Be ratio as calculated in DR model for $z_h = 4kpc$, lower curve – interstellar, upper curve – modulated. Data: Ulysses (Connell 1998), Voyager (Lukasiak et al. 1999), ACE (Binns et al. 1999), ISOMAX (Hams et al. 2001; de Nolfo et al. 2001).
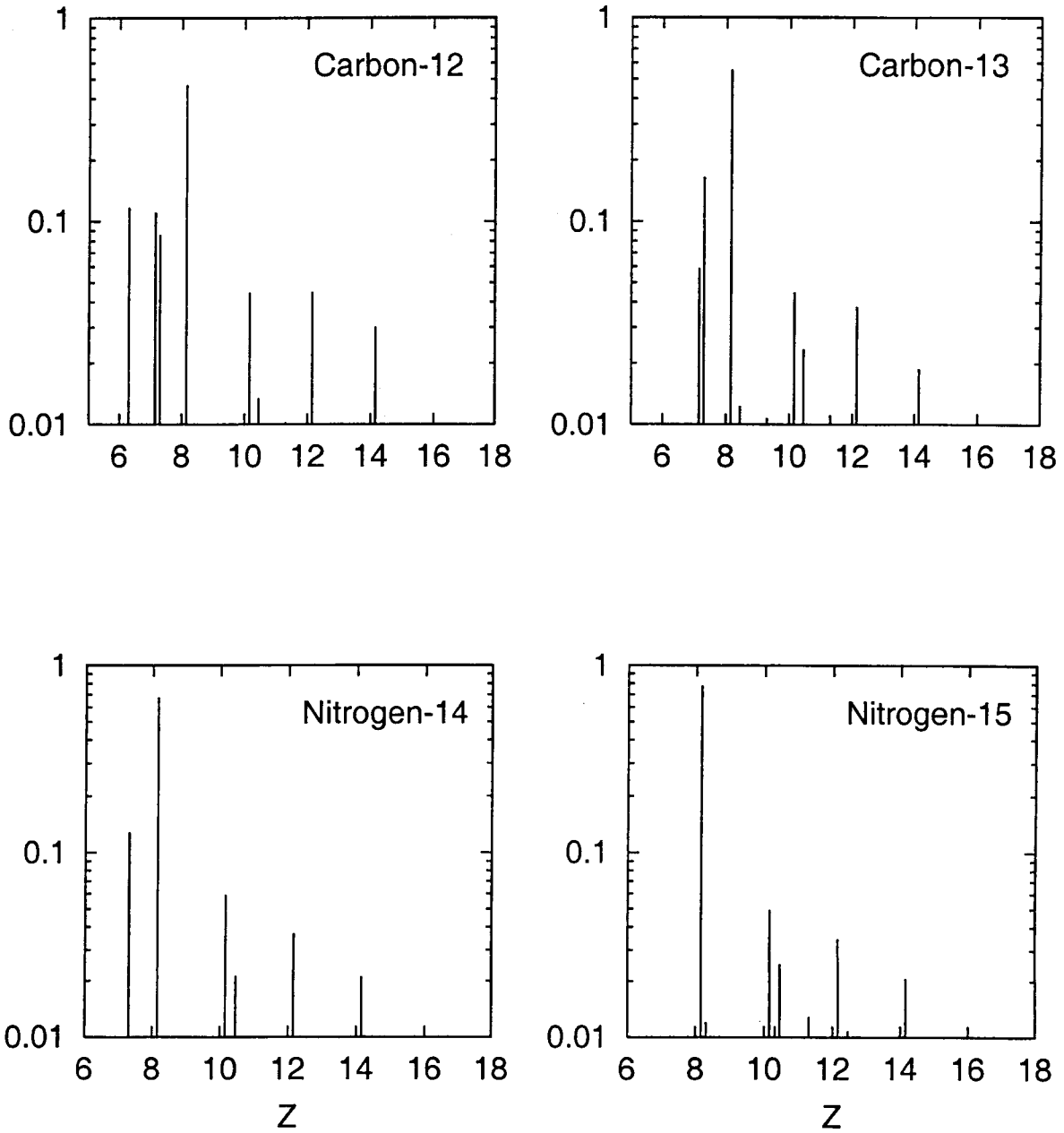
Fig. 15.— Contributions of isotopes to production of Carbon and Nitrogen. The cumulative production cross sections of Carbon and Nitrogen isotopes weighted with the flux of corresponding primary isotope in CR at 2 GeV/nucleon are shown vs. nucleus charge Z. The contributions of isotopes of a given element are indicated by separate lines.